Evaluation of the accuracy of the RDG approximation for the absorption and scattering properties of fractal aggregates of flame-generated soot

Liu, Fengshan; Snelling, David

Publisher's version / Version de l'éditeur:

Proceedings of the 40th Thermophysics Conference, 2008, 2008

40th Thermophysics Conference
23 - 26 June 2008, Seattle, Washington

AIAA 2008-4362

Evaluation of the Accuracy of the RDG Approximation for the Absorption and Scattering Properties of Fractal Aggregates of Flame-Generated Soot

Fengshan Liu, David R. Snelling
Institute for Chemical Process and Environmental Technology, National Research Council
Building M-9, 1200 Montreal Road, Ottawa, Ontario, Canada K1A 0R6

The accuracy of the Rayleigh-Debye-Gans approximation for the absorption and scattering properties of fractal aggregates of soot was evaluated against the generalized multi-sphere Mie solution, which is the most accurate solution technique for the optical properties of non-overlapping spherical particle systems. The fractal aggregates investigated in this study contain from 5 to 893 primary particles of 30 nm in diameter. These fractal aggregates were numerically generated using a combination of the particle-cluster and cluster-cluster aggregation algorithms with specified fractal properties. The wavelengths considered are 1064 nm and 532 nm and the corresponding size parameters of primary particle are 0.089 and 0.177, respectively. The Rayeligh-Debye-Gans approximation underestimates the aggregate absorption and total scattering cross section areas by approximately 10%, depending on the aggregate size. The generalized multi-sphere Mie-solution predicts oscillatory variation of the normalized *vv* scattering cross section at large scattering angles, rather than the exponential decay predicted by the Rayleigh-Debye-Gans theory. The generalized multi-sphere Mie-solution also predicts different forward-to-backward *vv* scattering ratios of large aggregates than the Rayleigh-Debye-Gans theory.

I. Introduction

KNOWLEDGE of the absorption and scattering properties of flame-generated soot is not only important to quantify the contribution of soot to thermal radiation transfer in flames, fires, and combustion systems, but is also essential in many optically based diagnostic techniques for measurements of soot properties, such as volume fraction and morphology (primary particle diameter and aggregate size). For example, the absorption cross section of soot aggregates is required to calculate the laser energy absorption rate and the thermal radiation intensity in laser-induced incandescence (LII) techniques when the effect of soot particle aggregation is taken into account [1,2] and the scattering properties are required in multi-angle laser elastic scattering techniques for soot morphology measurements [3,4].

Experimental evidence indicates that the primary soot particle diameters fall in the range 10 to 60 nm for most combustion sources, and thus can be reasonably assumed to be in the Rayleigh regime in the visible spectrum. Soot generated in flames forms fractal aggregates containing nearly spherical primary particles, as a result of cluster-cluster aggregation [5,6]. Within any given aggregates, the sizes of primary particle have a narrow distribution and can be approximately treated as identical in diameter [6]. Although there is a small degree of overlapping or necking between two neighboring primary particles, it is reasonable to assume that primary particles are in point-contact [6], which is an assumption commonly made in almost all theoretical and numerical studies of the optical properties of soot aggregates.

The structure of soot aggregates can be described as mass fractal [5]. Due to such rather complex structure of soot aggregates, their optical properties cannot be adequately described by the Rayleigh approximation or the Mie solution for the volume based equivalent sphere [7,8], since the rather open structure of soot aggregate cannot be represented by a compact sphere. Several studies, e.g. [9,10], have established that the optical properties of fractal aggregates can be evaluated by the Rayleigh-Debye-Gans theory for fractal aggregates (RDG-FA) with reasonable accuracy. The study of Van-Hulle et al. [11], however, showed that the RDG-FA approximation predicts very poor results of total scattering cross sections compared to more accurate results based on the discrete dipole approximation (DDA) and the generalized Mie-solution method (GMM). GMM was referred to as the rigorous solution (RS) in [11].

Many previous numerical studies have been devoted to quantifying the accuracy of the RDG-FA approximation for the absorption and scattering cross sections of flame-generated soot over a relatively wide range of primary particle size parameter and aggregate size, see [8-11] and the references cited therein. These studies suffer one of the following two drawbacks. In some studies, such as [9], the soot aggregates were numerically generated using the cluster/cluster aggregation algorithm of Jullien and Botet [12]. As a result, the fractal parameters of these numerical aggregates fell in a relatively wide range, rather than fixed at the desired values. For example, Farias et al. [9] reported that the numerical aggregates they generated have fractal dimensions in the range of 1.6 to 1.9 for aggregate size $N > 48$. Consequently, the numerical results of the optical properties of different aggregate sizes are affected by the variation in the fractal parameters. Although these results are relevant for comparison with experimental data, they are not ideal for evaluating the accuracy of the RDG-FA approximation due to the variation of fractal parameters from one aggregate to another. Other evaluation studies rely on the volume integral equation formulation (VIEF) [9] or the coupled electric and magnetic dipole (CEMD) method [13,14]. It is worth pointing out that these are also approximate methods, albeit that they are believed to be more accurate than the RDG-FA theory. Results of IEFS and CEMD may not be adequate to evaluate the accuracy of the RDG-FA theory under certain conditions, especially for very large aggregates and/or large primary particle size parameters where the multiple scattering effect is significant and the individual primary particle may no longer be approximated as a point dipole.

It was observed more than a decade ago by Farias et al. [9] that numerical studies of the optical properties of soot before 1995 were not adequate for providing an quantitative evaluation of the accuracy of the RDG-FA scattering theory, since these studies either involved fundamentally accurate solutions for small aggregates where effects of multiple and self-induced scattering are small, or approximate solutions having uncertain accuracy for large soot aggregates. Although the situation has been improved somewhat due to the more recent studies of Farias et al. [9,10] using VIEF and the integral equation formulation for scattering (IEFS) and Van-Hulle et al. [11] using discrete dipole approximation (DDA) and GMM, further evaluation of the accuracy of RAG-FA theory is required for the reasons discussed above. Moreover, it is of importance to revisit this issue with the availability of the exact GMM method and the tunable particle-cluster and cluster-cluster aggregation algorithms for the generation of fractal aggregates with identical fractal parameters.

In this study, fractal soot aggregates containing from 5 to 893 identical primary particles of 30 nm in diameter were numerically generated using a combined cluster-particle aggregation and cluster-cluster aggregation algorithm for specified fractal parameters (fractal dimension and prefactor). As a result, the aggregates of different size have identical fractal parameters and the uncertainty due to the variation in the fractal parameters among aggregates of different size was removed. The other advantage of the present study, compared to most of the previous ones, lies in the method used to obtain the benchmark solutions for the evaluation of the RDG-FA approximation. The benchmark solutions were obtained using the GMM method developed by Xu [15,16]. GMM provides exact solutions for non-overlapping spherical particle systems and is not limited to small primary particle size parameters. Therefore, it is an ideal tool to study the optical properties of multi-sphere fractal aggregates. In addition, the present work evaluated soot aggregates as large as 893. However, due to the excessively large amount of memory required to run GMM for large aggregates and relatively large size parameter of primary particle and the limitations of available computing resources, the present evaluation study was limited to relatively small primary particle size parameters. Larger primary particle size parameters will be investigated in the near future as adequate computing resources become available.

II. Theory

A. Numerical Generation of Fractal Aggregates

Soot, like many other aerosols, is formed by the aggregation of small, nearly identical and spherical primary particles into complex geometries, which are quite open in structure and cannot be described adequately by a compact sphere or other simple shapes as far as their optical properties are concerned. The fractal-like structure of soot aggregates can be described by the following statistical scaling law [17]

$$N = k_f \left(\frac{R_g}{a} \right)^{D_f} \tag{1}$$

We employ the particle radius a, rather than the particle diameter d_p, as the length scale in Eq. (1), where N is the number of primary particles within the given aggregate, k_f and D_f are the prefactor and fractal dimension, respectively, and R_g is the radius of gyration defined as [18]

$$R_g^{\,2} = \frac{1}{N}\sum_{i=1}^{N}(\mathbf{r}_i - \mathbf{r}^0)^2 + a^2 \tag{2}$$

$$\mathbf{r}^0 = \frac{1}{N}\sum_{i=1}^{N}\mathbf{r}_i \tag{3}$$

where vectors $\mathbf{r}_i$ and $\mathbf{r}^0$ define the position of the *i*th primary particle centre and the centre of the aggregate, respectively.

Following the study of Filippov et al. [18], small soot aggregates (up to N = 31) were generated numerically using the tunable particle-cluster aggregation or the sequential algorithm (SA). In this algorithm, identical spherical particles are added one by one, to an existing aggregate (cluster) starting from a smallest aggregate containing 3 primary particles. The newly added primary particle to the existing aggregate of size (N-1) obey the following two rules: (i) it is in point-touch (no overlapping and no gap) with one of the primary particles in the aggregate and the touching point is randomly determined, and (ii) the newly generated larger aggregate always satisfy the scaling law, Eq.(1), exactly. These requirements are guaranteed by ensuring the position of the centre of the newly added particle $\mathbf{r}_N$ satisfies the following equation, which is derived from the definition of the radius of gyration, Eqs. (2) and (3), and the scaling law, Eq. (1), for the existing (size N-1) and the new (size N) aggregates [18]

$$(\mathbf{r}_N - \mathbf{r}^0{}_{N-1})^2 = \frac{N^2a^2}{N-1}\left(\frac{N}{k_f}\right)^{2/D_f} - \frac{Na^2}{N-1} - Na^2\left(\frac{N-1}{k_f}\right)^{2/D_f} \tag{4}$$

where $\mathbf{r}^0{}_{N-1}$ is the centre of the existing aggregate of size N-1. Eq.(4) indicates that the centre of the newly added particle must be placed on the surface of a sphere whose centre is at $\mathbf{r}^0{}_{N-1}$ and whose radius is the square root of the right hand side of Eq. (4). To fulfill the first condition, the distance between the centre of the newly added primary particle and one of the primary particles in the existing aggregate must be 2a, i.e.,

$$(\mathbf{r}_N - \mathbf{r}_j)^2 = 4a^2 \tag{5}$$

where $\mathbf{r}_j$ represents the centre of the jth primary particle in the existing aggregate. In our implementation of the sequential algorithm, the particle index j is first selected sequentially from the list of 1, 2, 3, …, N-1 (one at a time). Once $\mathbf{r}_j$ is known by selecting j, Eqs. (4) and (5) are solved for two of the three Cartesian coordinates of the centre of the particle to be added to the existing aggregate, with the other one, e.g. z_N, chosen randomly first. If there are no solutions to Eqs. (4) or (5) for the chosen value of z_N, a new value of z_N is chosen until real solutions to Eqs. (4) and (5) are obtained. To ensure there is no overlap of the newly added particle at $\mathbf{r}_N$ with any of the particles in the existing aggregate, the distance between $\mathbf{r}_N$ and the centre of all the other particles is calculated to make sure it is always greater than 2a. If overlap occurs, the particle index j is increased by 1 and the above procedure is repeated until all the required conditions are satisfied.

This algorithm is used to generate progressively larger aggregates up to N = 31. There are many aggregate configurations that generate a given size aggregate and obey the required conditions. Many different small aggregates were first generated by this particle-cluster (sequential) algorithm. In this study, we used typical fractal parameters of k_f = 2.3 and D_f = 1.78 for flame-generated soot and a fixed value of the primary particle radius of a = 15 nm (d_p = 30 nm). These small aggregates were then used to generate even larger aggregates using the cluster-cluster aggregation algorithm described below. Two typical SA generated aggregates of size N = 31 are displayed in Fig.1. These aggregates do not exhibit the highly ramified structure or the certain symmetry features observed by Filippov et al. [18]. Perhaps these aggregates are too small to display the characteristics observed by Filippov et al. Although there is no limitation to the size of aggregate this algorithm can generate, it is preferred not to use SA to generate very large aggregates. It has been shown by Filippov et al. [18] that the correlation function of aggregates generated using the particle-cluster method (SA) displays a slope that is different from that expected from the specified fractal dimension for the generation of these aggregates. Consequently, systematic errors can occur if these aggregates are used to study the physical

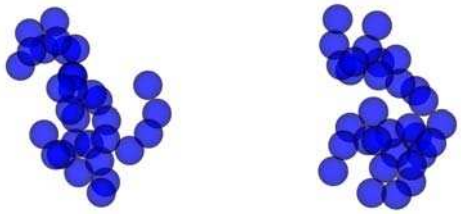

Figure 1. Two typical SA generated aggregates of N = 31 with d_p = 30 nm, D_f =1.78, and k_f = 2.3.

properties of fractal aggregates. On the other hand, Filippov et al. [18] also showed that correlation function for aggregates generated by the tunable cluster-cluster aggregation algorithm (CCA) do exhibit a consistent slope as expected from the specified fractal dimension. Therefore, CCA described below was used to create larger aggregates ($N > 31$) by merging two smaller aggregates generated using SA or CCA.

The tunable cluster-cluster aggregation algorithm shares many similarities with SA. When two existing smaller aggregates of size N_1 and N_2, whose radii of gyration are R_{g1} and R_{g2} respectively, are to be merged to generate a larger aggregate of size N_1+N_2, the following relation can be derived from the definition of R_g given in Eq. (2), [18]

$$(N_1 + N_2)R_g{}^2 = N_1 R_{g1}{}^2 + N_2 R_{g2}{}^2 + \frac{N_1 N_2}{N_1 + N_2}\Gamma^2 \tag{6}$$

where Γ is the distance between the geometrical centers of the two aggregates to be merged and R_g is the radius of gyration of the aggregate to be generated. Since the two smaller aggregates of size N_1 and N_2 and the bigger aggregate to be generated (size N_1+N_2) are all required to satisfy the scaling law, Eq. (1), the distance Γ in Eq. (6) can be re-written as [18]

$$\Gamma^2 = \frac{a^2(N_1 + N_2)}{N_1 N_2}\left(\frac{N_1 + N_2}{k_f}\right)^{2/D_f} - \frac{N_1 + N_2}{N_2}R_{g1}{}^2 - \frac{N_1 + N_2}{N_1}R_{g2}{}^2 \tag{7}$$

Without losing generality, we assume $N_1 \geq N_2$ in the following discussion. Eq. (7) indicates that in the generation of a bigger aggregate the centre of aggregate of size N_2 must fall on a sphere whose centre is at the centre of the aggregate of size N_1 and whose radius is Γ.

Some details of our implementation of CCA are discussed below. Once the two smaller aggregates (hereafter AG1 and AG2) are available, the first step is to identify a primary particle within AG1, P1, and a primary particle within AG2, P2. Once P1 and P2 are identified, a translational operation is performed to AG2 in such a way that P2 is to be relocated at the position of P1. This operation ensures that the final aggregate to be generated satisfies the requirement that all the primary particles within it are in point touch if this requirement is fulfilled by both AG1 and AG2. However, it should be noted that the size of AG1 is reduced by 1 since P1 now is in complete overlap with P2. There are at least two methods to identify P1 and P2. The first method is to set P1 as the primary particle in AG1 which has the largest coordinate in a certain direction, such as in x direction. Correspondingly, P2 is the primary particle in AG2 which has the smallest coordinate in the same direction. The second method is to select P1 and P2 by visualizing AG1 and AG2 using graphical software, keeping in mind that P1 and P2 are always one of the primary particles residing on the outer perimeter of AG1 and AG2, respectively. The second step of CCA is to obtain the desired mass centre of AG2. Fig. 2 shows a schematic of CCA. In this figure, $\mathbf{r}_1^0$ represents the mass centre of AG1 (after removal of P1), $\mathbf{r}_C$ and $\mathbf{r}_2^{0,old}$ are

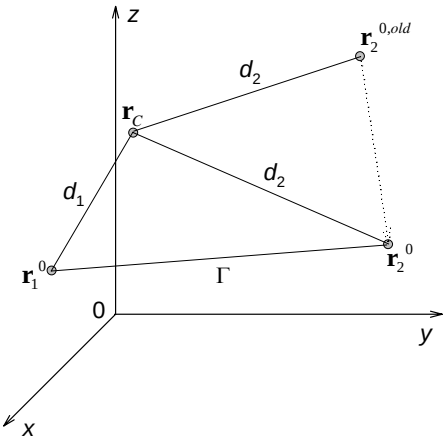

Figure 2. Schematic of the cluster-cluster aggregation algorithm.

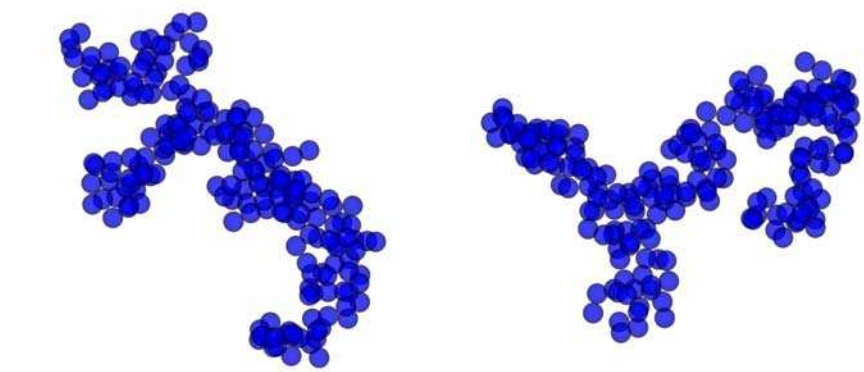

Figure 3. Two aggregates of size 199 generated using a combination of SA and CCA with d_p = 30 nm, D_f =1.78, and k_f = 2.3.

respectively the centre of P2 and the mass centre of AG2 after the translational operation of AG2, and $\mathbf{r}_2^{\,0}$ is the desired mass centre of AG2. The desired mass centre of AG2 must satisfy the following two conditions: (i) the distance between $\mathbf{r}_2^{\,0}$ and $\mathbf{r}_C$ is d_2, which is the same as that between $\mathbf{r}_2^{\,0,old}$ and $\mathbf{r}_C$, and (ii) the distance between $\mathbf{r}_2^{\,0}$ and $\mathbf{r}_1^{\,0}$ is Γ, which is governed by Eq. (7). Clearly the solution to $\mathbf{r}_2^{\,0}$ is not unique. The third step is to rotate AG2 in such a way that $\mathbf{r}_2^{\,0,old}$ is relocated at the new position $\mathbf{r}_2^{\,0}$. This step is shown in Fig. 2 by the dotted line. The fourth step is to check if there are overlapping primary particles among all the particles within the newly generated bigger aggregate. If overlapping occurs, the second step is repeated. Sometimes it is even necessary to restart the whole procedure by restarting the very first step. Two aggregates of size 199 generated using the combined SA and CCA are shown in Fig. 3.

Finally, it is worth point out that the tunable algorithms, either SA or CCA, proposed by Filippov et al. [18] can be used to generate any given aggregate size, i.e., there is no restriction to the value of *N*.

B. Rayleigh-Debye-Gans Fractal Aggregate Theory

When applied to fractal aggregates formed from identical primary particles, the validity of the RDG theory is based on following the assumptions [19,20]: (i) $|m-1|<<1$ and $2x_p|m-1|<<1$ with $m = n + ik$ being the refractive index of the particle material and $x_p = \pi d_p/\lambda$ the size parameter of primary particle, (ii) the effects of multiple scattering induced by other particles in the aggregate and self-interaction of the primary particle itself are negligible. These assumptions imply that each primary particle is in the Rayleigh regime and acts as a dipole source for scattered radiation. As pointed out by Köylü and Faeth [8,21], the first assumption is questionable for soot aggregate due to its relatively large refractive index. The theoretical estimate of Berry and Percival [22] based on a mean field theory showed that regardless its size *N* multiple scattering within a fractal aggregate can always be neglected as long as the fractal dimension D_f is less than 2. For this reason, Mulholland et al. [13] explicitly stated that the RDG approximation requires that the fractal dimension must be less than 2. Fortunately, all the experimental investigations reported in the literature on the morphology of soot generated from various combustion sources indicate that the fractal dimension of soot aggregates is always less than 2, which means that the structure of the aggregate is fairly open and the majority of the primary particles making up the aggregate is visible on a projected image, particulary for large aggregates.

Effects of multiple scattering within fractal aggregates with $D_f < 2$ have been shown to be significant by Nelson [23] using a mean field theory, by Mulholland et al. [13] using the CEMD method, and by Chen et al. [24] using the volume integral equation formulation, among others. Other attempts to provide quantitative evaluations of the RDG-FA approximation for the optical properties of soot aggregates have been made by various researchers, e.g. [9-11]. However, these studies suffer one of the two drawbacks discussed in the introduction.

The RDG-FA theory can be used to calculate the optical properties of fractal soot aggregates in the following two ways. One is to carry out detailed numerical calculations of the scattered field by using particle locations of the simulated aggregates and treating each primary particle as a dipole source [25,26]. The other is to directly employ the relatively simple and easy-to-use theoretical expressions of the RDG-FA approximation for the absorption and scattering cross sections of fractal aggregates given by Dobbins and Megaridis [27] and Köylü and Faeth [8,21]. The latter does not require the knowledge of the locations of individual primary particles, but requires the morphological information of the soot aggregate, including the fractal parameters (k_f and D_f), primary particle diameter d_p, and the aggregate size represented by *N*, besides the refractive index *m*. In this study, results of the RDG-FA approximation from the analytical expressions are compared against the exact solutions calculated using GMM. Here only the main theoretical results of the RDG-FA approximation are summarized. Detailed discussions of the assumptions and development of this theory can be found in [8,21,27].

Since primary particles are assumed in the Rayleigh limit, i.e., their size parameters x_p are less than 0.3, the optical cross sections of primary particles can be written as [21],

$$C_a^{\,p} = 4\pi x_p^{\,3} E(m)/k^2, \quad C_s^{\,p} = 8\pi x_p^{\,6} F(m)/(3k^2), \quad C_{vv}^{\,p} = x_p^{\,6} F(m)/k^2 \tag{8}$$

where $k = 2\pi/\lambda$ is the wave number, $E(m)$ and $F(m)$ are functions of the complex refractive index of soot *m* with $E(m) = \mathrm{Im}((m^2-1)/(m^2+2))$ and $F(m) = |(m^2-1)/(m^2+2)|^2$. Subscripts *a*, *s*, and *vv* represent absorption, scattering, and vertical (for incident radiation) and vertical (for scattered radiation) polarization. Superscript *p* indicates that the properties are for primary particles. Also $C_{hv}^{\,p} = C_{vh}^{\,p} \approx 0$ and $C_{hh}^{\,p} = C_{vv}^{\,p}\cos^2\theta$ with θ being the scattering angle formed between the scattered radiation direction and the incident radiation direction. Subscript *hh* indicates horizontal (for incident radiation)

and horizontal (for scattered radiation) quantities. In the RDG approximation, the scattering cross sections of an aggregate for polarized light are given as [21]

$$C_{vv}{}^{a}(\theta) = C_{hh}{}^{a}(\theta)/\cos^2\theta = N^2 C_{vv}{}^{p} f(qR_g) \tag{9}$$

where superscript a stands for aggregate, $q = 2k\sin(\theta/2)$ is the modulus of scattering vector and $f(qR_g)$ is the so-called aggregate form factor, which can be written in two different expressions in the small angle Guinier regime and in the large angle power-law regime, e.g. [21]. A unified approximate expression for $f(qR_g)$ valid in the entire range of qR_g has been recently introduced by Yang and Köylü [4]. Their expression for $f(qR_g)$ is written as

$$f(qR_g) = \left[1 + 8(qR_g)^2/(3D_f) + (qR_g)^8\right]^{-D_f/8} \tag{10}$$

The total scattering cross section can be written as [21]

$$C_s{}^{a} = N^2 C_s{}^{p} g(kR_g, D_f) \tag{11}$$

where the aggregate total scattering factor takes the following expression [21]

$$\begin{aligned} g(kR_g, D_f) &= 1 - 2(kR_g)^2/3, \quad \text{if } \beta = 3D_f/(8k^2R_g{}^2) \geq 1 \\ &= \frac{\beta}{2}(3 - 3\beta + 2\beta^2) - \frac{(kR_g\beta)^2}{3}(3 - 4\beta + 3\beta^2) + (2kR_g)^{-D_f}\left[\frac{3}{2 - D_f}\right. \\ &\left. - \frac{12}{(6 - D_f)(4 - D_f)} - 3\beta^{1 - D_f/2}\left(\frac{1}{2 - D_f} - \frac{2\beta}{4 - D_f} + \frac{2\beta^2}{6 - D_f}\right)\right], \quad \text{if } \beta < 1 \end{aligned} \tag{12}$$

The RDG-FA approximation has been commonly used to describe the absorption and scattering properties of fractal aggregates, especially for flame-generated soot, due to its simplicity, ease of use, and lack of better simple alternatives. The optical properties predicted by the above RDG-FA theory should be viewed as results averaged over a large number of aggregates of the same size for a given orientation and/or a large number of orientations for a given aggregate.

C. Generalized Mie-Solution Method

To quantify the accuracy of the RDG-FA approximation, it is crucial to establish exact solutions as a benchmark. In this study GMM was used for this purpose. GMM was developed by Xu [15,16] based on the framework of the Mie theory for a single sphere and the addition theorems for spherical vector wave functions. GMM provides rigorous and complete solution to non-overlapping multisphere light scattering problems and can be readily applied to soot aggregates. The key steps involved in the development of GMM include: (a) expansion of the scattered, internal, and incident electromagnetic fields in terms of vector spherical functions, (b) formation of a linear equation system through the boundary condition at each primary particles in the aggregate, (c) transformation of the waves scattered by an individual primary particle into the incident waves of the other particles in the aggregate through the addition theorems for vector spherical functions, and (d) solution of the linear system of interactive coefficients. The absorption and scattering cross sections and the four scattering matrix coefficients are analytically given by Xu [15,16]. It is clear that GMM rigorously accounts for the multiple scattering within the aggregate. GMM is extremely computationally demanding and memory intensive for large aggregates containing several hundreds of primary particles and when the size parameter of primary particle is large. The positions of primary particles for a given aggregate generated numerically are required in the execution of GMM. The GMM code provides the averaged scattering cross sections over all specified orientations. To our best knowledge, the study of Van-Hulle et al. [11] is the only one that made a quantitative evaluation of the RDG-FA theory using GMM results for soot aggregates containing up to 128 primary particles.

III. Results and Discussion

Numerical calculations were conducted for two wavelengths of 532 nm and 1064 nm, which are of great interest in LII applications. The refractive index of soot was assumed to be wavelength independent and equal to m =

1.6+0.6*i*, which is a typical value of soot in the visible. For a fixed value of primary diameter of d_p = 30 nm, the size parameters of primary particle, i.e., x_p = 0.177 at 532 nm and 0.0886 at 1064 nm, considered in this work are relatively small. Larger size parameters of primary particle are being investigated and will be reported in future publications. The results of GMM calculations were averaged over 1000 orientations. Selected cases were calculated over 8000 orientations and it was found that results averaged over 1000 and 8000 orientations are very close. For example, for N = 546 and λ = 532 nm it was found that the absorption and total scattering cross sections are within 0.5% of each other and the differences in the *vv* scattering cross section over all scattering angles are less than 2%.

A. Absorption and Total Scattering Cross Sections

Numerical results of absorption and total scattering cross sections for λ = 1064 nm and λ = 532 nm are summarized in Tables 1 and 2, respectively. It is clear that RDG-FA approximation in general underpredicts absorption and scattering by about 10%, depending on the aggregate size. It is observed that the largest relative error of the absorption cross sections predicted by the RDG-FA theory under the present conditions is just under 12%, Table 2, which is in agreement with the findings of Van-Hulle et al. [11] who also found that the RDG-FA theory underpredicts the absorption cross sections by about 10% under similar but not identical conditions. In addition, the absorption cross sections reported by Van-Hulle et al. [11] for *N* = 64 and 128 are also quantitatively comparable to our values given in Table 2. It is, however, very surprising to notice that Van-Hulle et al. [11] reported very large differences in the total scattering cross sections between the RDG-FA theory and GMM with about 60% for *N* = 64 and 150% for *N* = 128. Moreover, their total scattering cross sections calculated by GMM are consistently lower than those from RDG-FA. The present total scattering cross sections calculated by GMM are almost always higher than those from RDG-FA, except for the two largest aggregates at λ = 532 nm, Table 2. The present total scattering cross sections from GMM differ significantly not only quantitatively, but also qualitatively from those of Van-Hulle et al. in comparison to the results of RDG-FA. It is not clear about the causes of the substantially small total scattering cross sections calculated by GMM in the study of Van-Hulle et al. [11]. However, we would like to point out that the differences in the total scattering cross section calculated by GMM and RDG-FA shown in Tables 1 and 2 are similar to those reported by Farias et al. [9], who evaluated the RDG-FA theory using the volume integral equation formulation (VIEF) method of Iskander et al. [28].

Table 1. Absorption and total scattering cross sections at 1064 nm.

	Absorption, nm^2			Total scattering, nm^2		
N_p	GMM	RDG-FA	Error, %[a]	GMM	RDG-FA	Error, %[a]
5	356.255	338.218	-5.06	0.70921	0.68863	-2.90
10	720.187	676.436	-6.07	2.81533	2.71334	-3.62
20	1470.02	1352.87	-7.97	11.0746	10.4946	-5.24
50	3723.76	3382.18	-9.17	62.5316	58.1333	-7.03
100	7450.76	6764.36	-9.21	208.549	177.822	-14.73
150	11175.3	10146.54	-9.21	403.928	335.659	-16.90
199	14776.3	13461.08	-8.90	609.764	525.800	-13.77
348	25829.7	23539.98	-8.86	1309.88	1180.44	-9.88
546	40374.2	36933.41	-8.52	2337.40	2190.81	-6.27
893	65773.0	60405.74	-8.16	4516.26	4201.03	-6.98

[a] The relative error is defined as $(C_{RDG}-C_{GMM})/C_{GMM}\times 100\%$.

Table 2 Absorption and total scattering cross sections at 532 nm.

	Absorption, nm^2			Total scattering, nm^2		
N_p	GMM	RDG-FA	Error, %[a]	GMM	RDG-FA	Error, %[a]
5	740.429	676.436	-8.64	11.2313	10.5990	-5.63
10	1509.70	1352.87	-10.39	43.1458	39.7619	-7.84
20	3073.43	2705.74	-11.96	154.979	136.089	-12.19
50	7646.66	6764.36	-11.54	668.753	567.763	-15.10
100	15099.2	13528.7	-10.40	1732.90	1571.99	-9.29
150	22443.9	20293.1	-9.58	3004.99	2747.37	-8.57
199	29493.7	26922.2	-8.72	4276.25	4012.08	-6.18
348	50808.4	47078.0	-7.34	8437.07	8291.08	-1.73
546	79034.1	73866.8	-6.54	14260.9	14592.9	2.33
893	127610.0	120811.5	-5.33	25430.0	26605.0	4.62

[a] The relative error is defined as $(C_{RDG}-C_{GMM})/C_{GMM}\times 100\%$.

The absorption cross sections shown in Tables 1 and 2 are graphically displayed in Fig. 4 as values normalized by NC^{p}_{a} . Here the primary particle absorption cross section C^{p}_{a} is based on the Rayleigh regime expression given in Eq. (8). The normalized absorption cross section of the RDG-FA approximation remains constant at 1. Although the variation of the absorption cross section at 532 nm with the aggregate size *N* is more pronounced than that at 1064 nm, both curves exhibit the same overall trend. The absorption cross section first increases with increasing *N* to reach a peak value at an intermediate value of *N* then starts to decrease at even larger values of *N*. These results are qualitatively similar to those obtained previous by Nelson [23] using a mean field theory, Farias et al. [9] using VIEF of Iskander et al. [28], and Mulholland and Mountain [14] using the CEMD method. The present results, however, are superior to previous ones in terms of the consistency of the fractal properties from aggregate to aggregate and the accuracy of the benchmark solutions. The enhanced absorption for relatively small aggregates is attributed to the coupling between the electric fields of primary particles or the multiple scattering effect [13,14]. For even larger aggregates, the shielding effect, which reduces the absorption ability of the aggregate, becomes increasingly important and eventually results in the decrease in the absorption cross section. Such shielding effect can be observed either at large aggregate sizes for a given primary particle size parameter as shown in Fig. 1 and the results of Mulholland et al. [14] or at large primary particle size parameter for a given aggregate size [13]. The net effect of coupling and shielding is controlled by the relative importance of these two competing factors.

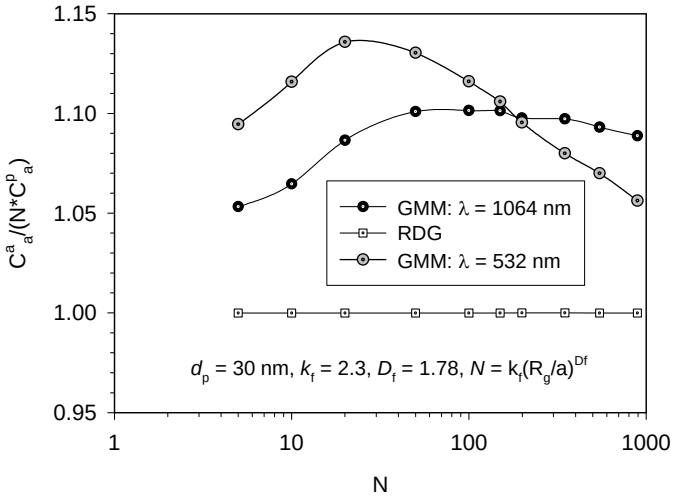

Figure 4. Comparison of the normalized absorption cross sections of soot aggregates at 532 nm and 1064 nm calculated using the RDG approximation and GMM.

The results shown in Fig. 4 indicate that the RDG-FA theory, which has been commonly used in LII studies, underestimates the aggregate absorption cross section by 5 to 13% for conditions typical to LII experiments conducted in laminar diffusion flames. Such deviation of the RDG-FA theory from the exact GMM solution could have serious implications for the calculated soot particle temperatures when the established value of E(m) is used or for the value of the soot absorption function E(m) determined from the low-fluence LII technique [1]. A detailed analysis of the effect of the soot aggregate absorption models, i.e., RDG-FA and GMM, on LII modeling is beyond the scope of this study.

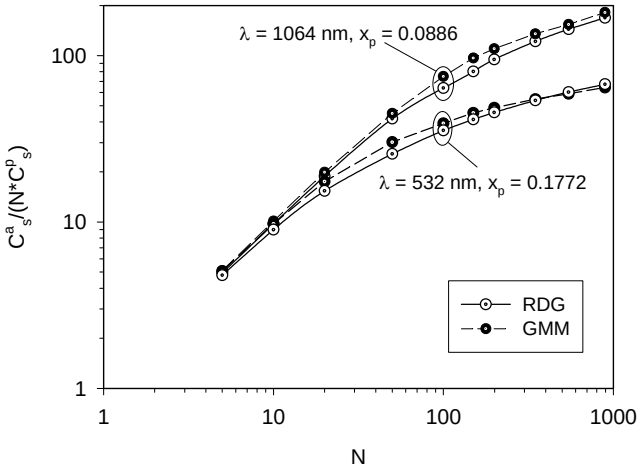

Figure 5. Comparison of the normalized total scatteringcross sections of soot aggregatesat 532 nm and 1064 nm calculated using the RDG approximation and GMM.

The normalized total scattering cross sections as a function of the aggregate size *N* are compared in Fig. 5. For relatively small aggregates, up to about 40 at λ = 1064 nm and up to about 10 at λ = 532 nm, the normalized total scattering cross section increases linearly with *N*. This is the expected behavior of the total scattering cross section, since for relatively small aggregates the scattered waves are essentially in phase and the total scattered intensity is proportional to N^2 [29]. With increasing *N* the normalized total scattering cross sections increase sublinearly. These

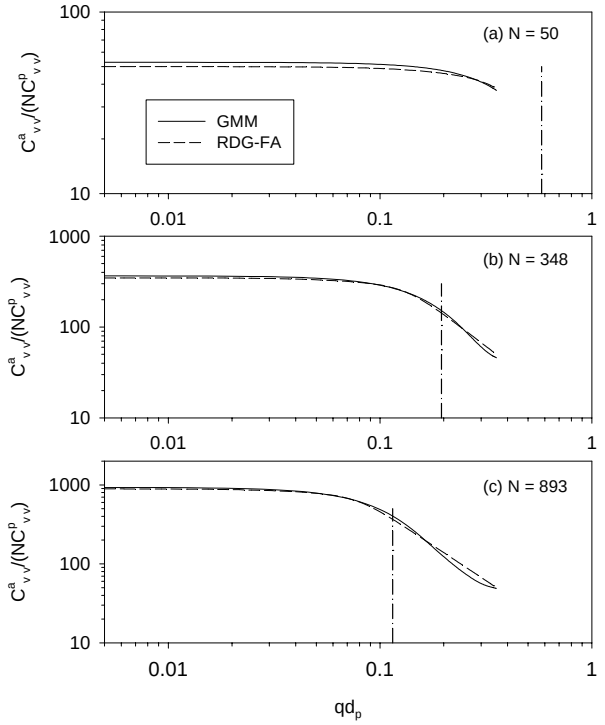

Figure 6. Normalized vv scattering cross sections as a function of qd_p for three aggregate sizes at λ = 1064 nm.

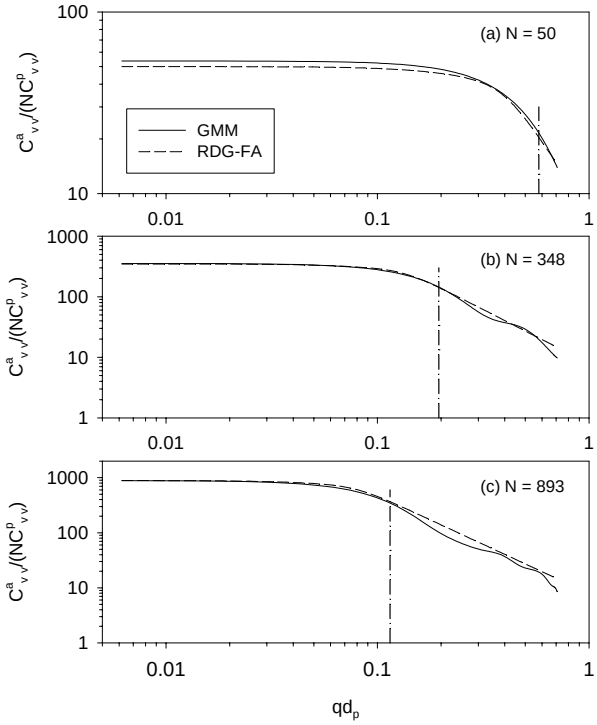

Figure 7. Normalized vv scattering cross sections as a function of qd_p for three aggregate sizes at λ = 532 nm.

results are also in qualitative agreement with the theoretical analysis of Sorensen [29] and the numerical calculations of Farias et al. [9]. It is also expected that the normalized total scattering cross sections saturate at sufficiently large N for fractal aggregates with $D_f < 2$ [9,22,27]. This behavior is somewhat more evident at λ = 532 nm than at λ = 1064 nm. It is clear from Fig. 5 that the saturation has not been reached for the aggregate sizes considered here. Similar to the results shown in Fig. 4 for the absorption cross section, the RDG-FA theory in general underpredicts the total scattering cross section. Although the present differences between the RDG-FA and GMM in the total scattering cross section are qualitatively similar to those between VIEF and RDG-FA results shown by Farias et al. [9], larger discrepancies between RDG-FA results and the benchmark than the previous ones are clearly seen from Fig. 5, suggesting that the present methodology is superior to those used in previous studies to provide more accurate quantitative evaluation of the accuracy of the RDG-FA theory.

B. Differential Scattering Cross Sections

Following Farias et al. [9], we compare GMM and RDG-FA results of the normalized vertical-vertical (*vv*) scattering cross section $C^a_{vv}(\theta)/(NC^p_{vv})$ as a function of the radiation momentum qd_p in Figs. 6 and 7 for λ = 1064 nm and λ = 532 nm, respectively. The vertical dash-dot lines in these figures represent the boundary between the Guinier regime and the power-law regime define as $qR_g = (3D_f/2)^{1/2}$ [21]. The RDG-FA results shown in Figs. 6 and 7 display extended Guinier regime under the conditions considered, especially at λ = 1064 nm where the power-law regime is not reached at N = 50, Fig. 6(a). At the shorter wavelength of λ = 532 nm, the power-law regime is reached for a larger range of the scattering angle. At small values of qd_p, the RDG-FA theory, Eqs. (9) and (10), predicts that the normalized *vv* scattering cross section is simply N. In the power-law regime, the normalized *vv* scattering cross section is independent of the aggregate size N, since it can be easily shown that $C^a_{vv}/(NC^p_{vv}) = 2^{D_f} k_f (qd_p)^{-D_f}$ in this regime. In the Guinier regime, the RDG-FA results are smaller than GMM results. However, the differences are less than 7%. In the power-law regime, the errors of the RD-FA results can be as high as 22% at λ = 1064 nm and 71% at λ = 532 nm reached for the largest aggregate considered at large scattering angles, Figs. 6(c) and 7(c). In addition, the GMM results in the power-law regime do not exhibit a linear decay on the log-log plot, suggesting that the normalized *vv* scattering cross section is not strictly an exponential function of qd_p. This is more pronounced at λ = 532 nm where the normalized *vv* scattering cross sections from

GMM exhibit oscillatory variation with qd_p, Figs. 7(b) and 7(c). To our best knowledge this oscillatory variation of the normalized *vv* scattering cross section at large scattering angles and sufficiently large primary particle size parameters has not been reported in the literature. This point deserves further research attention. It is worth pointing out that the GMM results shown so far, including those in Figs. 6 and 7, are based on a single aggregate realization for a given aggregate size but averaged over at least 1000 orientations. It has been shown by Farias et al. [9] that both aggregate and orientation averaging are important to the *vv* scattering cross section at large scattering angles. The importance of aggregate arrangement to differential scattering cross sections at an intermediate aggregate size of N = 199 is discussed in the next section.

A simple way to relate the *vv* scattering cross sections to the morphology of soot aggregates under investigation is to determine the forward-to-backward ratio as used by Yang and Köylü [4]. The forward-to-backward ratios, $R = C^a_{vv}(30°)/C^a_{vv}(150°)$, as a function of the aggregate size N calculated by GMM and RDG-FA are compared in Fig. 8. At the smaller primary particle size parameter, i.e., λ = 1064 nm, the ratios R calculated by GMM and RDG-FA increase monotonically with the aggregate size. However, the RDG-FA predicts smaller ratios at large aggregate sizes. The implication is that for an experimentally detected forward-to-backward scattering ratio the RDG-FA theory would return a larger aggregate size when it is used to interpret the experimental observation. For the larger primary particle size parameter considered, i.e., λ = 532 nm, on the other hand, GMM predicts a non-monotonic variation of the forward-to-backward scattering ratio with N at large aggregate sizes while the ratio from the RDG-FA theory saturates. Under conditions where the RDG-FA ratio does not saturate, the RDG-FA theory once again returns a much larger aggregate size for a given forward-to-backward scattering ratio. When the RDG-FA ratio saturates, Fig. 8 suggests that the RDG-FA theory should not be used to interpret the experimental observation, since the resultant aggregate size can be completely wrong. Moreover, the non-monotonic variation of R with N at large aggregate sizes predicted by GMM suggests that it is questionable to relate the forward-to-backward scattering ratio to the morphology of fractal soot aggregates under conditions where this ratio varies non-monotonically with the aggregate size. However, it should be pointed out that the non-monotonic variation of R with N at large aggregate sizes is a direct consequence of the oscillatory variation of the normalized *vv* scattering cross section at large scattering angles shown in Fig. 7.

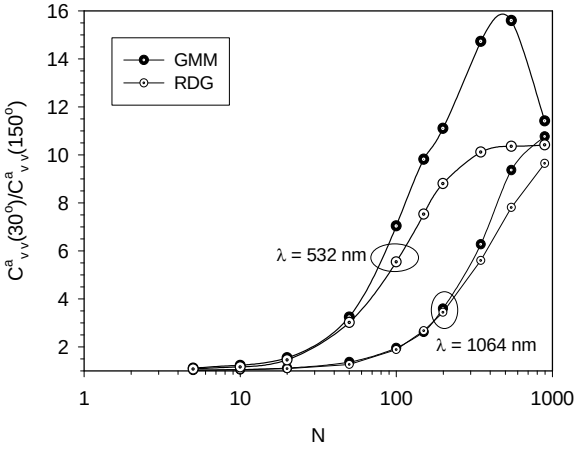

Figure 8. Variation of the forward-to-backward *vv* scattering cross sections ratio with the aggregate size.

C. Effect of Averaging over Aggregate Realization

As mentioned earlier, the GMM results presented so far are based on a single aggregate realization but averaged over at least 1000 orientations. It has been shown in previous studies that to obtain statistically meaningful results it is important to average the numerical results over both orientation [9,25] and aggregate realization [9], especially for scattering properties at large scattering angles. In this section the effect of aggregate realization on the numerical results of GMM was investigated for an aggregate size of N = 199 using 6 different aggregate realizations. All the results presented below are averaged over 8000 orientations.

Table 3 Absorption and total scattering cross sections at 1064 nm for 6 aggregates containing 199 primary particles.

Aggregates	Absorption nm^2	Total scattering nm^2	Absorption relative error, %	Scattering relative error, %
1	14776.3	609.764	0.323	-0.950
2	14776.3	619.807	0.323	0.682
3	14711.0	605.426	-0.120	-1.655
4	14716.5	607.652	-0.083	-1.293
5	14679.1	620.829	-0.337	0.848
6	14713.2	630.187	-0.105	2.368
mean	14728.7	615.611		

The orientation averaged absorption and total scattering cross sections of the six aggregates of N = 199 at λ = 1064 nm and 532 nm are summarized in Tables 3 and 4, respectively. For the absorption cross section, the effect of aggregate realization is fairly small, being less than 0.5% at both wavelengths. Although the variation of the total scattering cross section with the aggregate realization is larger than the absorption one, it still remains reasonably small, i.e., less than about 4%. These findings are in agreement with those made by Farias et al. [9].

Table 4 Absorption and total scattering cross sections at 532 nm for 6 aggregates containing 199 primary particles.

Aggregates	Absorption nm^2	Total scattering nm^2	Absorption relative error, %	Scattering relative error, %
1	29493.7	4276.25	0.259	-0.723
2	29409.4	4481.01	-0.028	4.030
3	29507.9	4287.20	0.307	-0.469
4	29434.3	4277.02	0.057	-0.706
5	29352.8	4221.25	-0.220	-2.000
6	29307.2	4301.73	-0.375	-0.132
Mean	29417.6	4307.41		

The effect of aggregate realization on the differential scattering cross sections at λ = 532 nm are shown in Figs. 9 and 10. Also plotted on these figures are the results of RDG-FA for comparison. It is evident that the aggregate structure affects the differential scattering cross properties at large scattering angles, similar to that shown by Farias et al. [9] in their VIEF calculations. At small scattering angles, however, the differential scattering properties is independent of the aggregate realization. The somewhat overprediction of the differential scattering properties by the RDG-FA theory at large scattering angles shown in Figs. 9 and 10 is also in qualitative agreement with that found by Farias et al. [9]. It is important to realize that all the six aggregates numerically generated here using the combined SA and CCA algorithm satisfy exactly the fractal relationship, Eq. (1), with identical fractal parameters k_f and D_f. Yet they still exhibit different differential scattering properties at large scattering angles. Therefore, it is clear that the optical properties of a given fractal aggregate are only largely, but not completely, governed by the morphological parameters, including k_f, D_f, d_p, and N. The more subtle difference in the structure of fractal aggregates of identical morphology affects their optical properties to a lesser degree. Although it is not clear on how such subtle difference in the structure among these fractal aggregates should be characterized, possible quantities to be investigated include the inertia tensor and the spatial distribution of pairs of particles [25]. Overall, the results shown in Tables 3 and 4 and Figs. 9 and 10 demonstrate that the effect of averaging over aggregate realization is fairly small.

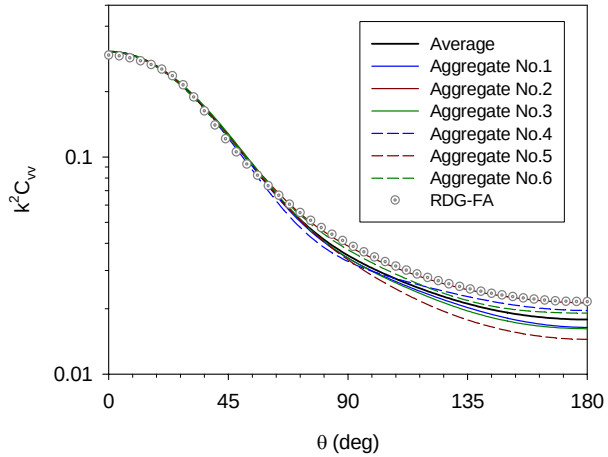

Figure 9. Effect of aggregate realization for N = 199 on the normalized *vv* scattering cross section at λ = 532 nm.

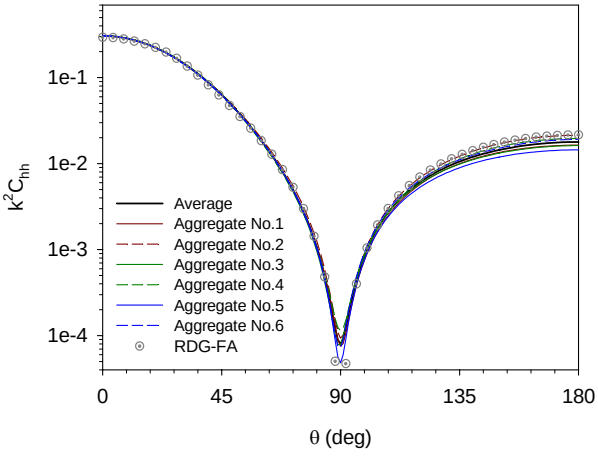

Figure 10. Effect of aggregate realization for N = 199 on the normalized *hh* scattering cross section at λ = 532 nm.

IV. Conclusion

The absorption and scattering properties of fractal soot aggregates were calculated using the RDG-FA approximation and the exact generalized multi-sphere Mie-solution method. GMM calculations were conducted using numerically generated fractal aggregates by a combination of tunable particle-cluster and cluster-cluster aggregation algorithms. These numerical aggregates satisfy exactly the specified fractal parameters. Therefore, the present results do not suffer uncertainties caused either by variation in the fractal parameters of different sized aggregates or the accuracy of the method for generating the benchmark solutions. The following conclusions can be drawn from the present numerical study:

1. Under the conditions of this study, RDG-FA predictions are in overall reasonable agreement with those from GMM. The present numerical results provide more accurate quantification of the accuracy of the RDG-FA theory in the prediction of fractal soot aggregates.
2. The RDG-FA theory underpredicts the absorption cross sections by about 10%. For LII applications, however, such underprediction of the absorption cross section by the RDG-FA approximation is not acceptable. Further studies are required to quantify the consequences of using the RDG-FA approximation in LII modelling.
3. The normalized *vv* scattering cross section calculated by GMM exhibits an oscillatory variation at large scattering angles, rather than the exponential decay predicted by the RDG-FA theory.
4. The RDG-FA theory predicts smaller forward-to-backward *vv* scattering cross section ratios than GMM. The ratios predicted by RDG-FA also saturate at large aggregates. The non-monotonic variation of the forward-to-backward *vv* scattering ratio at large aggregates predicted by GMM raises question about the effectiveness of using this ratio to infer the morphology of the soot aggregates to be interrogated.

Further studies are required to extend the size parameter of the primary particle to larger values and to confirm the oscillatory variation of the *vv* scattering cross section through further investigation of the effect of averaging over aggregate realizations for large aggregates.

Acknowledgments

We would like to thank Dr. Y.-L. Xu for making his GMM computer codes available. The GMM Fortran code used in this study, gmm01f.f, was downloaded from the following website:
http://www.astro.ufl.edu/~xu/codes/gmm01f.

References

[1]Snelling, D. R., Liu, F., Smallwood, G. J., and Gülder, Ö. L., "Determination of the soot absorption function and thermal accommodation coefficient using low-fluence LII in a laminar coflow ethylene diffusion flame," *Combust. Flame*, Vol. 136, 2004, pp. 180-190.

[2]Liu, F., Yang, M., Hill, F. A., Snelling, G. J., and Smallwood, G. J., "Influence of polydisperse distributions of both primary particle and aggregate size on soot temperature in low-fluence LII," *Appl. Phys. B*, Vol. 83, 2006, pp. 383-395.

[3]Köylü, Ü. Ö., "Quantitative analysis of in situ optical diagnostics for inferring particle/aggregate parameters in flames: implications for soot surface growth and total emissivity," *Combust. Flame*, Vol. 109, 1996, pp. 488-500.

[4]Yang, B., and Köylü, Ü. Ö., "Soot processes in a strongly radiating turbulent flame from laser scattering/extinction experiments," *JQSRT*, Vol. 93, 2005, pp. 289-299.

[5]Megaridis, C. M., and Dobbins, R. A., "Morphological description of flame-generated materials," *Combust. Sci. Tech.*, Vol. 71, 1990, pp. 95-109.

[6]Faeth, G. M., and Köylü, Ü. Ö., "Soot morphology and optical properties in nonpremixed turbulent flame environments," *Combust. Sci. Tech.*, Vol. 108, 1995, pp. 207-229.

[7]Dalzell, W. H., Williams, G. C., and Hottel, H. C., "A light-scattering method for soot concentration measurements," *Combust. Flame*, Vol. 14, 1970, pp. 161-170.

[8]Köylü, Ü. Ö., and Faeth, G. M., "Radiative properties of flame-generated soot," *J. Heat Transfer*, Vol. 115, 1993, pp. 409-417.

[9]Farias, T. L., Carvalho, M. G., Köylü, Ü. Ö., and Faeth, G. M., "Computational evaluation of approximate Rayleigh-Debye-Gans/fractal-aggregate theory for the absorption and scattering properties of soot," *J. heat Transfer*, Vol. 117, 1995, pp. 152-159.

[10]Farias, T. L., Köylü, Ü. Ö., and Carvalho, M. G., "Range of validity of the Rayleigh-Debyre-Gans theory for optics of fractal aggregates," *Applied Optics*, Vol. 35, No. 33, 1996, pp. 6560-6567.

[11]Van-Hulle, P., Weill, M.-E., Talbaut, M., and Coppalle, A., "Comparison of numerical studies characterizing optical properties of soot aggregates for improved EXSCA measurements," *Part. Part. Syst. Charact.*, Vol. 19, 2002, pp. 47-57.

[12]Jullien, R., and Botet, R., *Aggregation and Fractal Aggregates*, World Scientific Publishing Co., Singapore, 1987, pp. 46-60.

[13]Mulholland, G. W., Bohren, C. F., and Fuller, K. A., "Light Scattering by Agglomerates: Coupled Electric and Magnetic Dipole Method," *Langmuir*, Vol. 10, 1994, pp. 2533-2546.
[14]Mulholland, G. W., and Mountain, R. D., "Coupled Dipole Calculation of Extinction Coefficient and Polarised Ratio for Smoke Agglomerates," *Combust. Flame*, Vol. 119, 1999, pp. 56-68.
[15]Xu, Y.-L., "Electromagnetic scattering by an aggregate of spheres," *Applied Optics*, Vol. 34, No. 21, 1995, pp. 4573-4588
[16]Xu, Y.-L., "Electromagnetic scattering by an aggregate of spheres: far field," *Applied Optics*, Vol. 36, No. 36, 1997, pp. 9496-9508.
[17]Forrest, S. R., and Witten Jr., T. A., "Long-range correlations in smoke-particle aggregates," *J. Phys. A: Math. Gen.*, Vol. 12, No. 5, 1979, pp. L109-L117.
[18]Filippov, A. V., Zurita, M., and Rosner, D. E., "Fractal-like aggregates: relation between morphology and physical properties," *J. Colloid Interface Sci.*, Vol. 229, 2000, pp. 261-273.
[19]Bohren, C. F., and Huffman, D. R., *Absorption and Scattering of Light by Small Particles*, Wiley, New York, 1983, pp. 158-165.
[20]Kerker, M., *The Scattering of Light*, Academic Press, New York, 1969, pp. 414-486.
[21]Köylü, Ü. Ö., and Faeth, G. M., "Optical Properties of Overfire Soot in Buoyant Turbulent Diffusion Flames at Long Residence Time," *J. Heat Transfer*, Vol. 116, 1994, pp. 152-159.
[22]Berry, M. V., and Percival, I. C., "Optics of Fractal Clusters such as Smoke," *Optica Acta*, Vol. 33, No. 5, 1986, pp. 577-591.
[23]Nelson, J., "Test of a Mean Field Theory for the Optics of Fractal Clusters," *J. Modern Optics*, Vol. 36, No. 8, 1989, pp. 1031-1057.
[24]Chen, H. Y., Iskander, M. F., and Penner, J. E., "Light Scattering and Absorption by Fractal Agglomerates and Coagulations of Smoke Aerosols," *J. Modern Optics*, Vol. 37, No. 2., 1990, pp. 171-181.
[25]Mountain, R. D., and Mulholland, G. W., "Light Scattering from Simulated Smoke Agglomerates," *Langmuir*, Vol. 4, 1988, pp. 1321-1326.
[26]Farias, T. L., Köylü, Ü. Ö., and Carvalho, M. G., "Effects of Polydispersity of Aggregates and Primary Particles on Radiative Properties of Simulated Soot," *JQSRT*, Vol. 55, No.3, 1996, pp. 357-371.
[27]Dobbins, R. A., and Megaridis, C. M., "Absorption and Scattering of Light by Polydisperse Aggregates," *Applied Optics,* Vol. 30, No. 33, 1991, pp. 4747-4754.
[28]Iskander, M. F., Chen, H. Y., and Penner, J. E., "Optical Scattering and Absorption by Branched Chains of Aerosols," *Applied Optics*, Vol. 28, No. 15, 1989, pp. 3083-3091.
[29]Sorensen, C. M., "Light Scattering by Fractal Aggregates: A Review," *Aerosol Sci. Tech.*, Vol. 35, 2001, pp. 648-687.